Dosimetric measurements of an *n*-butyl cyanoacrylate embolization material for arteriovenous malformations

Zacariah E. Labby[a)]
Department of Human Oncology, University of Wisconsin–Madison, 600 Highland Avenue, Madison, Wisconsin 53792

Neeraj Chaudhary
Division of Neurointerventional Radiology, Departments of Radiology and Neurosurgery, University of Michigan Hospital and Health Systems, 1500 East Medical Center Drive, Ann Arbor, Michigan 48109

Joseph J. Gemmete
Division of Neurointerventional Radiology, Departments of Radiology, Neurosurgery, and Otolaryngology, University of Michigan Hospital and Health Systems, 1500 East Medical Center Drive, Ann Arbor, Michigan 48109

Aditya S. Pandey
Department of Neurosurgery, University of Michigan Hospital and Health Systems, 1500 East Medical Center Drive, Ann Arbor, Michigan 48109

Donald A. Roberts
Radiation Physics Division, Department of Radiation Oncology, University of Michigan Hospital and Health Systems, 1500 East Medical Center Drive, Ann Arbor, Michigan 48109

(Received 28 October 2014; revised 16 February 2015; accepted for publication 22 February 2015; published 18 March 2015)

Purpose: The therapeutic regimen for cranial arteriovenous malformations often involves both stereotactic radiosurgery and endovascular embolization. Embolization agents may contain tantalum or other contrast agents to assist the neurointerventionalists, leading to concerns regarding the dosimetric effects of these agents. This study investigated dosimetric properties of *n*-butyl cyanoacrylate (*n*-BCA) plus lipiodol with and without tantalum powder.
Methods: The embolization agents were provided cured from the manufacturer with and without added tantalum. Attenuation measurements were made for the samples and compared to the attenuation of a solid water substitute using a 6 MV photon beam. Effective linear attenuation coefficients (ELAC) were derived from attenuation measurements made using a portal imager and derived sample thickness maps projected in an identical geometry. Probable dosimetric errors for calculations in which the embolized regions are overridden with the properties of water were calculated using the ELAC values. Interface effects were investigated using a parallel plate ion chamber placed at set distances below fixed samples. Finally, Hounsfield units (HU) were measured using a stereotactic radiosurgery CT protocol, and more appropriate HU values were derived from the ELAC results and the CT scanner's HU calibration curve.
Results: The ELAC was 0.0516 ± 0.0063 cm^{-1} and 0.0580 ± 0.0091 cm^{-1} for *n*-BCA without and with tantalum, respectively, compared to 0.0487 ± 0.0009 cm^{-1} for the water substitute. Dose calculations with the embolized region set to be water equivalent in the treatment planning system would result in errors of −0.29% and −0.93% per cm thickness of *n*-BCA without and with tantalum, respectively. Interface effects compared to water were small in magnitude and limited in distance for both embolization materials. CT values at 120 kVp were 2082 and 2358 HU for *n*-BCA without and with tantalum, respectively; dosimetrically appropriate HU values were estimated to be 79 and 199 HU, respectively.
Conclusions: The dosimetric properties of the embolization agents are very close to those of water for a 6 MV beam. Therefore, treating the entire intracranial space as uniform in composition will result in less than 1% dosimetric error for *n*-BCA emboli smaller than 3.4 cm without added tantalum and *n*-BCA emboli smaller than 1.1 cm with added tantalum. Furthermore, when effective embolization can be achieved by the neurointerventionalist using *n*-BCA without tantalum, the dosimetric impact of overriding material properties will be lessened. However, due to the high attenuation of embolization agents with and without added tantalum for diagnostic energies, artifacts may occur that necessitate additional imaging to accurately identify the spatial extent of the region to be treated.
 [http://dx.doi.org/10.1118/1.4915080]

Key words: arteriovenous malformations, stereotactic radiosurgery

1. INTRODUCTION

Arteriovenous malformations (AVMs) are collections of abnormal arteries and veins (and the resulting nidus) that do not connect through the normal intervening capillary bed. Cerebral AVMs are often discovered after an intracerebral hemorrhage, the risk of which has been shown to be between 2% and 4% annually.[1,2] The combined morbidity and mortality per bleed event can approach 50%.[3]

The therapeutic regimen for cranial AVMs often involves both stereotactic radiosurgery and endovascular embolization, with the goal of eventual complete obliteration of the AVM nidus due to embolization and scarring. Two common commercially available embolization agents are Onyx (ethylene-vinyl alcohol copolymer) and *n*-butyl cyanoacrylate (*n*-BCA). The Onyx material comes with added tantalum ($Z = 73$) powder to aid neurointerventional radiologists in visualization on fluoroscopy during embolization, and the *n*-BCA agents can be cured with iodinated oil (lipiodol) and can also have tantalum powder added.

Published reports have suggested lower obliteration rates after neoadjuvant embolization[4–7] and raised concerns as to the dosimetric effects of embolization agents with added high-Z materials.[8,9] Partly in answer to these reports, a study was published by Roberts *et al.*[10] that quantified the dosimetric effects of Onyx on therapeutic-energy radiation. Onyx embolization agents of two different viscosity levels were found to have clinically negligible dosimetric consequences for smaller effective thickness values, with down-stream transmission reduced by up to 10% for ≥2 cm thicknesses of Onyx. The present report aims to apply similar methodology to quantify the dosimetric consequences of a commercially available *n*-BCA embolization agent cured with lipiodol, both with and without the addition of tantalum powder.

2. METHODS AND MATERIALS

As *n*-BCA is a type of glue, it needs to be cured before it will set and solidify. In the human body, blood is the main curing agent, though oil may be mixed into the *n*-BCA for curing purposes. For this study, the two samples of *n*-BCA were provided from the manufacturer (Codman Trufill; Codman & Shurtleff, Inc., Raynham, MA) cured with lipiodol, a poppy seed oil containing iodine ($Z = 53$), one with and one without added tantalum. These samples will be denoted as *n*-BCA-Ta and *n*-BCA, respectively. The samples were approximately 10 cm in diameter and 5 mm thick. A figure of the *n*-BCA sample is shown in Fig. 1.

2.A. Imaging studies

The *n*-BCA and *n*-BCA-Ta samples were imaged using a CT simulator (Philips Big Bore CT scanner; Philips Medical Systems, Cleveland, OH) using modified versions of an SRS imaging protocol (1 mm contiguous slices, 400 mAs, 90, 120, or 140 kVp). The samples were sandwiched between two 5 cm slabs of Solid Water (Gammex, Middleton, WI). Average Hounsfield unit (HU) values were acquired in a central 7 cm diameter circular ROI using 5 mm averaged coronal slices through the center of the samples. Using the scanner's HU-to-electron density table, generated at time of CT scanner commissioning, we calculated the apparent electron densities for Solid Water, *n*-BCA, and *n*-BCA-Ta from the tabulated HU values.

FIG. 1. Photograph of the cured *n*-BCA sample provided by the manufacturer.

Additionally, the samples were imaged in a water bath using a 3T MR system (Siemens Skyra) using both a standard $T1$-weighted pulse sequence and a time-of-flight pulse sequence (typical for AVM patients) to evaluate image quality with the embolization agents.

2.B. Effective linear attenuation measurements

A 6 MV photon beam was used from a Varian Clinac EX (Varian Medical Systems, Palo Alto, CA) to measure attenuation of the *n*-BCA samples and of Solid Water. Higher energy measurements were not made, since SRS procedures use the 6 MV photon beam in many clinics. In the previous report by Roberts *et al.*,[10] transmission measurements were made using an ionization chamber and Solid Water. Linear attenuation coefficients were calculated from the transmission and measured thickness. However, the *n*-BCA samples exhibited heterogeneous thickness readings across the sample diameter (see Fig. 1). Linear attenuation coefficients derived using similar methodology to Roberts *et al.* resulted in unacceptably large error bars on attenuation coefficients due to the large variability in sample thickness.

For this study, attenuation coefficients were calculated using transmission maps made from the ratio of portal images from the Linac's MV imager panel. The 6 MV image of the sample was divided by a 6 MV image of an open field of identical dimensions. For imaging purposes, the *n*-BCA samples were suspended using plastic wrap halfway between the radiation source and the imager panel. The resulting ratio between the image of the sample and the open field image characterized the transmission across the sample disc.

The thickness of each sample was mapped by ray-tracing the CT scans of the *n*-BCA samples after thresholding. Thresholding was applied such that HU values above 1000 were classified as sample, and HU values below 1000 were classified as nonsample. This particular threshold value was derived from HU value line profiles through the samples and

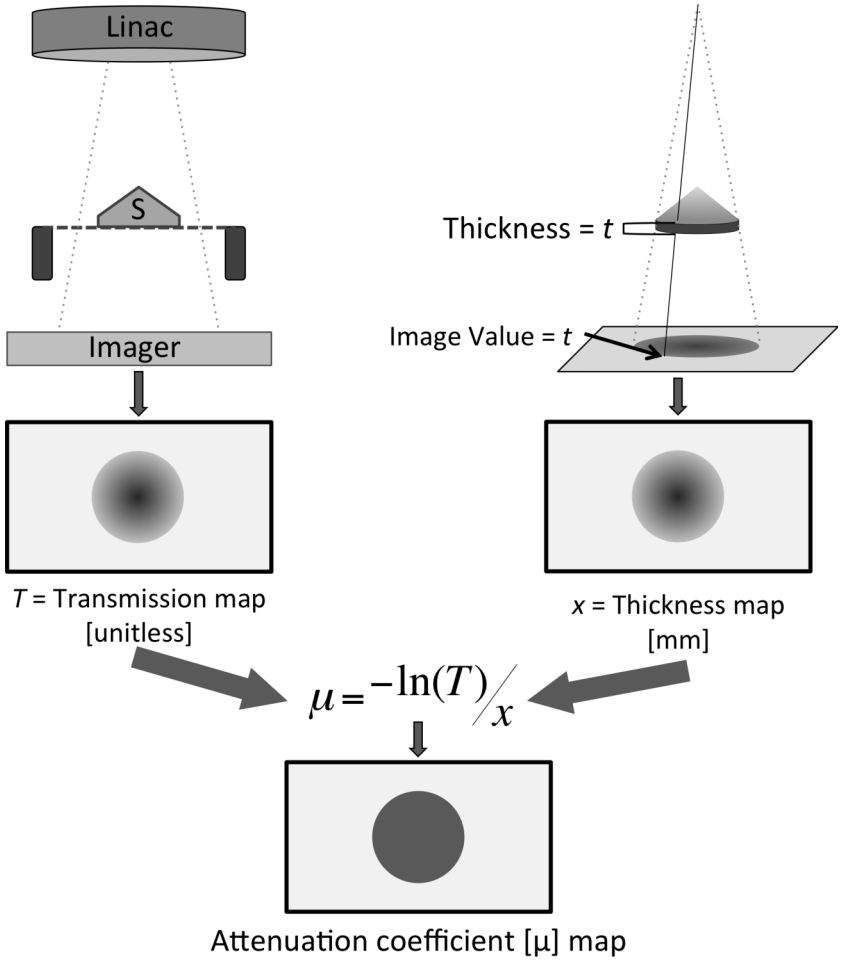

FIG. 2. Graphical description of the process used to calculate linear attenuation coefficient maps. Left side: transmission maps are generated by acquiring an MV image of the sample (S) using a 6 MV Linac beam and normalizing to an open field. Right side: thickness maps are generated by ray tracing through the masked 3D CT dataset from a virtual source under identical geometry to the transmission map measurements. The two maps are combined to form the attenuation coefficient (μ) map.

visual identification of where the sample started and stopped. The segmentation process was insensitive to the exact value of the threshold. The resulting segmented sample volume was virtually projected in a cone-beam geometry onto an image matrix identically sized to the actual acquired portal images (same pixel pitch, same source-to-imager distance, etc.). The thickness was derived by multiplying this projected sum image by the oblique voxel thickness as a function of off-axis position.

The two images (thickness map and transmission map) were manually registered by point matching to visible landmarks (such as cracks) in the samples using the freely available software ImageJ (version 1.48, http://imagej.nih.gov/ij/). After registration, the linear attenuation coefficient μ was calculated using the standard formula (see Fig. 2). The uncertainty in μ was calculated using spatial statistics in manual regions of interest.

2.C. Dosimetric deviations from homogeneous calculations

Based on the effective linear attenuation coefficients derived from the above analysis, the dosimetric consequence can be calculated if one were to assume a homogeneous water-equivalent composition inside the embolization material. Due to the streak artifacts sometimes observed in the proximity of these embolization agents, users may be tempted to override the density inside the embolized volume with that of water or to simply perform all dose calculations without density correction. In reality, while the *n*-BCA samples have slightly higher attenuation than water, their attenuation properties in a 6 MV beam are not accurately represented by their apparent HU value from a diagnostic energy CT image. The presence of high atomic number additives (iodine is present in both samples, and tantalum is present in the *n*-BCA-Ta sample) leads to increased photoelectric interaction, whereas MV interactions are predominantly Compton-based.

The dosimetric deviations for assumed homogeneous densities were calculated by taking the transmission ratio of an identical thickness of embolization material with that of Solid Water. If the attenuation of a certain thickness of embolization agent is greater than that of water, the dose deviation will be a negative value; the "true dose" will be less than that reported by the homogeneous dose calculation. Uncertainties on this dose deviation are calculated by propagating the error found in the linear attenuation coefficient measurements. Note

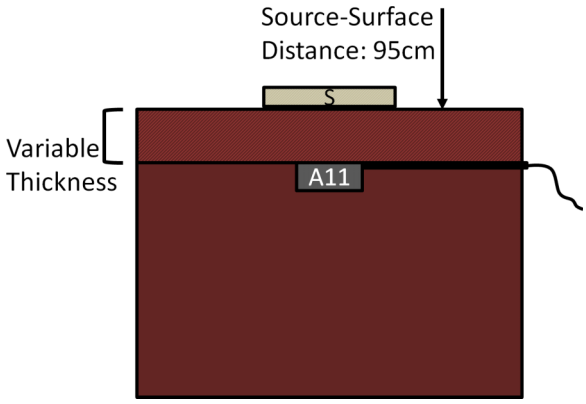

FIG. 3. Experimental setup for measuring interface effects. The parallel plate chamber ("*A*11") was placed below the sample *S* (*n*-BCA, *n*-BCA-Ta, or Solid Water) and a variable thickness of Solid Water.

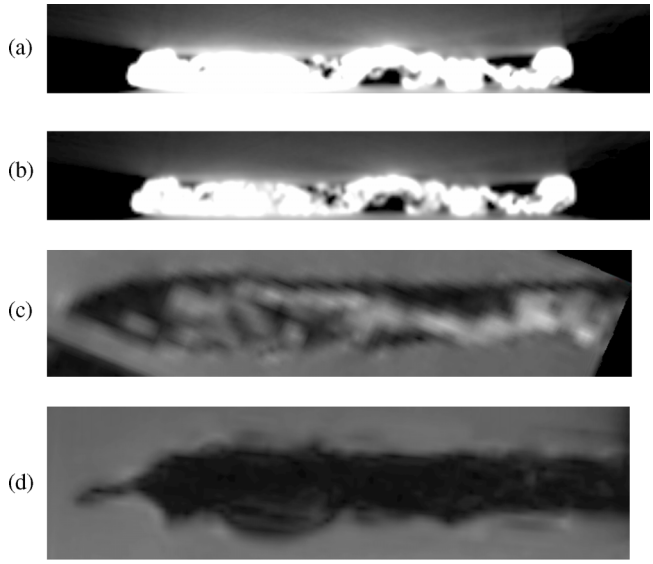

FIG. 4. Images of the *n*-BCA sample. (a) Axial CT view with window set to [−1000,1000] HU, (b) same as (a), except with window [−1000,2500] HU, (c) sample sealed in a plastic bag, submerged in water, and imaged using a *T*1-weighted MR protocol, and (d) sample imaged using a time-of-flight MR protocol (typical for AVM patients). The slight apparent artifacts around the sample in (d) are likely due to air trapped in plastic bag.

that this particular experiment only refers to dose deviations due to overriding the density of the embolization agent itself, not including any deviations that may arise when setting the entire patient volume to water-equivalent material (e.g., not accounting for bony anatomy).

2.D. Interface effects

Interface effects were investigated using a parallel plate ion chamber (Exradin A11; Standard Imaging, Middleton, WI) placed below the various samples and a variable thickness of Solid Water. The experimental setup is shown in Fig. 3. The sample "*S*" (*n*-BCA, *n*-BCA-Ta, or a 1 cm Solid Water piece) was placed on top of a variable thickness of Solid Water, and the whole setup was irradiated with a 5×5 cm field size (enough to fully encompass the ionization chamber but not excessively irradiate the stem). Measurements using the *n*-BCA samples were compared to measurements using the Solid Water piece as the sample *S* to calculate the relative enhancement from the presence of the embolization agent. Prior to this comparison, the measurements acquired with the 1 cm Solid Water piece as the sample *S* were corrected using TPR ratios to derive measurements that would have been acquired with a Solid Water sample piece equal in thickness to the *n*-BCA samples. The net uncertainty in the interface effect calculation included all relevant measurement uncertainty, as well as uncertainty from the *n*-BCA sample thicknesses used in the TPR corrections mentioned above.

3. RESULTS

Imaging results from the *n*-BCA samples are shown in Fig. 4. Streaks can be seen emanating from the samples in the CT images, but the MR images appear largely artifact-free except for some slight susceptibility artifact on the periphery of the sample, where some air was trapped in the plastic bag used to protect the sample from the surrounding water bath. The extracted HU values, along with apparent relative electron densities from our scanner's HU-to-electron density curve, are given in Table I.

Figure 5 shows the transmission map of the *n*-BCA sample, along with the projected thickness map and the derived linear attenuation coefficient map. Both the thickness map and transmission map generation techniques were validated to within 2% using Solid Water samples under identical geometry conditions to the *n*-BCA samples. Figure 5(c) shows some nonuniformity in regions of low thickness; we believe that the sample is not rigidly stable in regions of very low thickness and we therefore excluded those regions from our linear attenuation coefficient extraction. The linear attenuation coefficient results are shown in Table II.

TABLE I. Extracted HU values and apparent relative electron densities from CT scans of *n*-BCA samples and Solid Water.

	90 kVp		120 kVp		140 kVp	
Material	HU ± SD	ρ_e (relative)	HU ± SD	ρ_e (relative)	HU ± SD	ρ_e (relative)
Solid Water	28 ± 9	1.05	24 ± 9	1.05	34 ± 10	1.06
n-BCA	2285 ± 1012	2.44	2082 ± 880	2.31	2119 ± 797	2.34
n-BCA-Ta	2339 ± 950	2.47	2358 ± 913	2.49	2233 ± 812	2.41

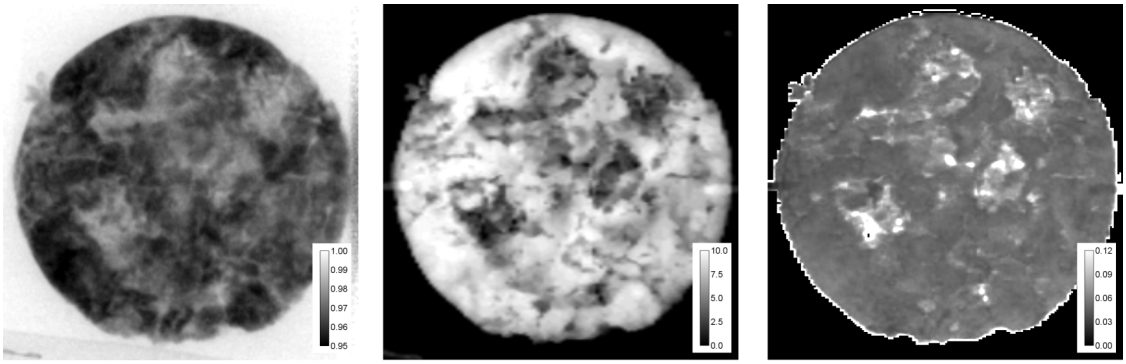

(a) (b) (c)

FIG. 5. Property maps of the *n*-BCA sample. (a) Transmission map (unitless), (b) projected thickness map in millimeters, and (c) derived linear attenuation coefficient map (unitless).

TABLE II. Linear attenuation coefficients of materials measured in this study.

Material	Linear attenuation coefficient μ (cm^{-1})
Liquid water[a]	0.04942
Solid Water	0.0487 ± 0.0009
n-BCA	0.0516 ± 0.0063
n-BCA-Ta	0.0580 ± 0.0091

[a]The liquid water attenuation coefficient is given only for reference and was taken from NIST Physical Reference Data (http://physics.nist.gov/PhysRefData/XrayMassCoef/ComTab/water.html).

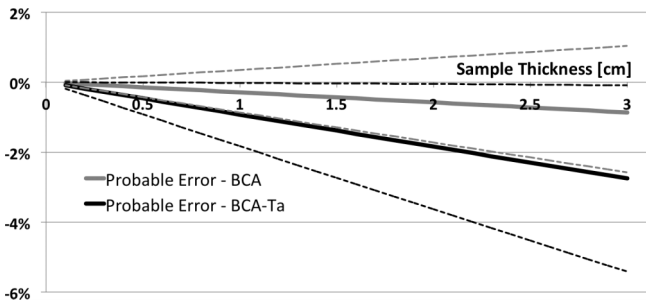

FIG. 6. Probable error in dose calculation resulting from assignment of water-equivalent density to the embolization agents. Negative values indicate that the true dose with the embolization agent present would be lower than that calculated with water-equivalent density. Dashed lines are one standard deviation.

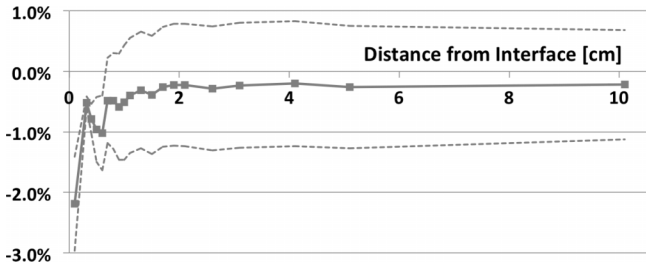

FIG. 7. Relative enhancement over water from the *n*-BCA embolization agent. For experimental setup, see Fig. 3. The dashed lines are single standard deviation error bars.

We also calculated the "appropriate HU values" for the embolization agents (that is, the HU values that would appropriately represent the 6 MV attenuation characteristics of the samples). As Compton interactions are proportional to electron density, we used the ratios of attenuation coefficients in Table II and the known density of Solid Water to calculate that the appropriate (relative) electron density is 1.11 and 1.25 for *n*-BCA and *n*-BCA-Ta, respectively. Using the inverse of the HU-to-electron density curve for our CT scanner, we found the appropriate HU values to be 79 ± 120 HU for the *n*-BCA sample and 199 ± 172 HU for the *n*-BCA-Ta sample.

Based on the linear attenuation properties of the *n*-BCA embolization agents, the dosimetric discrepancy introduced by overriding the embolization material with water-equivalent density is shown in Fig. 6. Since the point estimate of μ for the embolization agents is larger than that of Solid Water, the true dose when the embolization agents are present will be lower than the dose calculated under the assumption that the embolization agents are water-equivalent. Such dose calculations would result in errors of −0.29% and −0.93% per cm thickness of embolization agent without and with tantalum, respectively.

The interface effects for the *n*-BCA sample are quantified in Fig. 7. The relative enhancement over water in Fig. 7 was taken as the difference of the measurement ratio from unity. Within the first few millimeters, the interface enhancement quickly approaches zero (within the measurement uncertainty). The plot for the *n*-BCA-Ta sample exhibited similar behavior, but the deviation from null enhancement in the first few millimeters is less pronounced.

4. DISCUSSION AND CONCLUSIONS

This study investigated the dosimetric effects of two embolization agents used in arteriovenous malformations. Both embolization agents are made from *n*-BCA cured with an iodinated oil, one with and one without added tantalum powder. While the dosimetric properties of other embolization agents (i.e., Onyx) have been investigated previously,[10] this work represents the first dosimetric study of *n*-BCA embolization materials. The materials in this study showed markedly

less attenuation at 6 MV beam energies than Onyx materials (e.g., compare Table II in this study to Fig. 7 in the report by Roberts *et al.*) with interface effects of similar magnitude. Simple attenuation measurement techniques, such as bulk attenuation measurements at a single or small set of measurement points below a sample, were not used in this study due to the texture inherent in the cured *n*-BCA samples (see Fig. 1). Instead, a thickness mapping technique was developed for this work, and the resulting attenuation map of the sample appeared to be robust outside of very thin sample regions. Very thin sections of the samples were, for lack of a better word, crumbly.

This study provides effective attenuation coefficients for *n*-BCA embolization agents for a 6 MV beam, as well as quantifies the interface effects in the immediate proximity of the embolization agents. For first-order effects due to attenuation differences, the abscissa of Fig. 6 was chosen to represent the range of typical AVM masses (1–3 cm), where the probable error peaks at −0.87% and −2.75% for *n*-BCA samples without and with tantalum, respectively. As shown in Fig. 7, the dose on the distal (downstream) interface of the embolization material is slightly lower than that for an equivalent amount of water replacing the embolization agent. The same effect is observed for both *n*-BCA and *n*-BCA-Ta, though the effect is more pronounced with *n*-BCA. The observed deficit could be explained by increased attenuation and the rebuildup of electron fluence past the interface with the textured sample (see Fig. 1), though no matter the cause, the magnitude of the interface effect is below the threshold of clinical relevance.

This work provides derived relative electron densities for the embolization agents, as well as HU values that could be used to override the densities assigned by the treatment planning system based on the CT scan alone. The HU values provided above are only strictly relevant for the HU-to-electron density curve associated with the CT scanner used in this study. Any readers interested in overriding regions of *n*-BCA embolization agents with dosimetrically appropriate image values are encouraged to either use the electron densities calculated above directly (if supported by the treatment planning system) or to find appropriate HU values based on the user's own CT scanner calibration curve.

With regards to the selection of *n*-BCA agents with and without tantalum, anecdotal feedback from some radiologists suggests that the addition of tantalum powder is not necessary for visualization during embolization on fluoroscopy. This finding suggests that *n*-BCA without tantalum could be used on a routine basis, thereby mitigating the increased dosimetric discrepancy observed with the addition of tantalum. Subjectively, the *n*-BCA without tantalum also exhibited fewer streak artifacts in the acquired CT scan. However, both *n*-BCA agents did exhibit at least some streaking in the CT images, and other reports have indicated that target delineation on CT can be made difficult by embolization agents with high atomic number components.[11] Image fusion with other imaging modalities (e.g., magnetic resonance imaging or angiography, CT angiography, etc.) is therefore recommended for appropriate delineation of target boundaries.

While the dosimetric effects of the *n*-BCA embolization agents in this study are small for a 6 MV beam, the discrepancies from standard water dosimetry are slightly larger for *n*-BCA with added tantalum. Data are provided in this report to understand the dosimetric consequences of the embolization agents, as well as to override the values of CT images in embolized regions with dosimetrically appropriate values. Finally, imaging studies showed that embolized regions may require imaging beyond CT (such as MRI) to appropriately identify targets obfuscated by streak artifacts.

[a]Author to whom correspondence should be addressed. Electronic mail: zelabby@humonc.wisc.edu

[1]D. L. Barrow and A. Reisner, "Natural history of intracranial aneurysms and vascular malformations," Clin. Neurosurg. **40**, 3–39 (1993).
[2]S. L. Ondra, H. Troupp, E. D. George, and K. Schwab, "The natural history of symptomatic arteriovenous malformations of the brain: A 24-year follow-up assessment," J. Neurosurg. **73**(3), 387–391 (1990).
[3]J. van Beijnum *et al.*, "Outcome after spontaneous and arteriovenous malformation-related intracerebral haemorrhage: Population-based studies," Brain **132**, 537–543 (2009).
[4]B. E. Pollock, J. C. Flickinger, L. D. Lunsford, A. Maitz, and D. Kondziolka, "Factors associated with successful arteriovenous malformation radiosurgery," Neurosurgery **42**(6), 1239–1244 (1998).
[5]B. E. Pollock, D. Kondziolka, L. D. Lunsford, D. Bissonette, and J. C. Flickinger, "Repeat stereotactic radiosurgery of arteriovenous malformations: Factors associated with incomplete obliteration," Neurosurgery **38**(2), 318–324 (1996).
[6]L. Miyawaki *et al.*, "Five year results of linac radiosurgery for arteriovenous malformations: Outcome for large AVMS," Int. J. Radiat. Oncol., Biol., Phys. **44**(5), 1089–1106 (1999).
[7]S. L. Blackburn *et al.*, "Combined endovascular embolization and stereotactic radiosurgery in the treatment of large arteriovenous malformations," J. Neurosurg. **114**(6), 1758–1767 (2011).
[8]Y. M. Andrade-Souza, M. Ramani, D. Scora, M. N. Tsao, K. terBrugge, and M. L. Schwartz, "Embolization before radiosurgery reduces the obliteration rate of arteriovenous malformations," Neurosurgery **60**(3), 443–451 (2007).
[9]Y. M. Andrade-Souza *et al.*, "Liquid embolisation material reduces the delivered radiation dose: A physical experiment," Acta Neurochir. **150**(2), 161–164 (2008).
[10]D. A. Roberts, J. M. Balter, N. Chaudhary, J. J. Gemmete, and A. S. Pandey, "Dosimetric measurements of Onyx embolization material for stereotactic radiosurgery," Med. Phys. **39**(11), 6672–6681 (2012).
[11]A. R. Plasencia and A. Santillan, "Embolization and radiosurgery for arteriovenous malformations," Surg. Neurol. Int. **3**(Suppl. 2), 90–104 (2012).